

INVESTIGATION OF SONIC JET MIXING IN A STREAM OF SUPERSONIC CROSS-FLOW USING LARGE EDDY SIMULATIONS

Zeeshan A. Rana , Dimitris Drikakis , Ben J. Thornber
Fluid Mechanics & Computational Sciences Group,
Department of Aerospace Sciences, Cranfield University,
Cranfield, Bedfordshire, MK43 0EB, UK

Keywords: *Jet Penetration, Jet Mixing, Scramjet Combustor, High-Resolution Methods*

Abstract

This paper presents an application of a finite volume Godunov-type implicit large eddy simulation (ILES) method to study a transverse sonic Jet Injection into a Supersonic Cross-flow (JISC) of turbulent flow. The ILES method is based on fifth-order in space and third-order in time numerical schemes along with a digital-filter-based turbulent inflow data generation method. The simulations are compared against experimental data and other computational results obtained from classical LES methods. Using the simulation results, the jet penetration and flow properties upstream and downstream the jet plume are investigated.

1 Introduction

In recent years, LES has made significant contributions towards understanding the physics of certain flows for which it is very difficult to carry out experiments. This is mainly due to efficiency of the LES codes and the computational resources available today. One such flow is the jet injection into a main stream cross-flow, where the main stream flow could be subsonic or supersonic. For the subsonic main stream flow case an important example is a jet emerging through a puncture in a gaseous tank at high pressure. On the other hand, an example of a supersonic main stream flow is inside a scramjet combustion chamber, where

the fuel is typically injected transversely to the main supersonic flow. Both of these flows require understanding of the flow mechanics/physics for proper design of the equipment. For both of the subsonic and supersonic examples, the underpinning knowledge of the jet entering a transverse flow is similar, therefore most of the theoretical and experimental studies of this phenomenon started with subsonic main flow and expanded to include supersonic main flows [17, 18]. Ultimately, the driving force behind these studies was to understand the fluid physics of sonic jet into a supersonic transverse flow. In 1958 Adamson & Nicholls [16] presented the internal structure of an under-expanded jet into quiescent air in order to study the structure of the jet and discussed a method to calculate the position of the Mach disc as the jet expands into the air. Due to the efforts in the mid 1950s and 1960s, the structure and mechanics of the jet injected into a supersonic cross-flow is reasonably well understood, as explained below.

Fig. 1(a) is a schematic diagram for a typical under-expanded sonic jet injected into a supersonic transverse stream along with a 3D schematic showing the structure of the shock-waves generated when the jet interacts with the cross-flow in Fig. 1(b). As the under-expanded jet enters the cross-flows, it expands through a Prandtl-Meyer expansion fan and at the same time deflects and turns its direction along the

main flow. Thus, the jet acts as an obstruction to the main supersonic cross-flow and generates a bow shock as shown in the Fig. 1. The boundary layer starts to separate just ahead of the bow shock and a small separation zone is visible which results in a smaller weak shock, called a lambda shock, that interacts with the stronger bow shock. This deflection and the size of the separation zone is mainly dependent upon the momentum of the main stream flow (for details see Schetz & Billig [20]). The jet emerges from the orifice and expands to the atmospheric pressure at the jet boundary. This constant pressure on the jet boundary causes it to bend towards the axis of flow and the barrel shock emerges. Due to the high pressure ratio of the flow, the barrel shock do not meet at the axis of flow but instead a normal shock is generated which has its centre at the axis of flow. This shock formation is termed a Mach disc. A small recirculation/separation zone is also visible immediately downstream of the jet. There is a horseshoe vortex which wraps around the jet column and forms wake vortices in the downstream. Further downstream the jet boundary takes the form of a pair of counter rotating vortices (CRV). All these separation zones, shocks and vortex structures give rise to a very complex flow downstream of the jet which is helpful for the mixing of the jet with the mainstream flow.

In 1966, Schetz & Billig[20] published an analysis of the gaseous jet injected transversely into a supersonic stream and introduced the jet-to-cross-flow momentum flux ratio (J) as the most important parameter in order to determine the jet penetration in the cross flow.

$$J \equiv \frac{\rho_j V_j^2}{\rho_c V_c^2} = \frac{\gamma_j P_j M_j^2}{\gamma_c P_c M_c^2} \quad (1)$$

where ρ , V , γ , P and M represent density, velocity, ratio of specific heats, pressure and Mach number, respectively; the subscripts j and c represent jet and cross-flow, respectively, and will be used throughout this paper. To devise an empirical correlation to determine the height of the jet penetration into the transverse flow, the following pa-

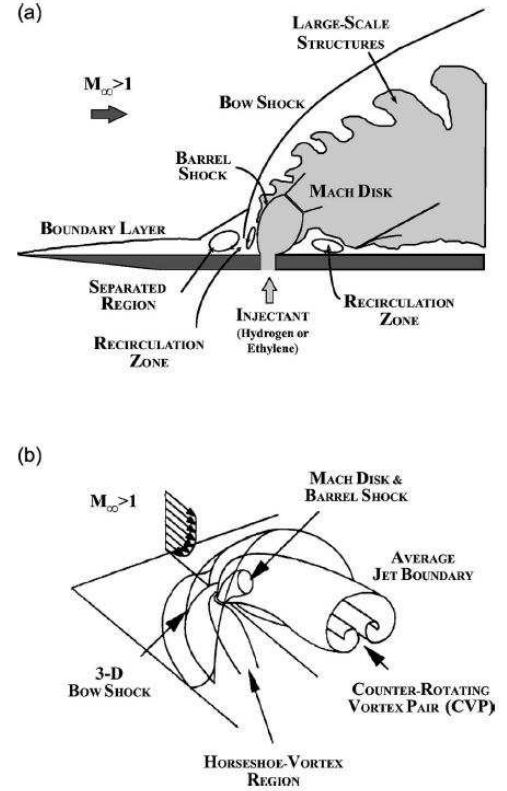


Fig. 1 Schematic diagram of a transverse jet into a supersonic cross flow (a) instantaneous, (b) 3D averaged flow features [14, 15]

rameter, proposed by Cohen *et al.* [19], has been used:

$$\frac{H_{mid}}{D} = \left[\frac{2 \left(1 + \frac{\gamma_j - 1}{2} M_j^2 \right)}{\gamma_j^2 M_j (\gamma_j + 1)} \right]^{0.25} \times \left[\frac{1.25 (1 + \gamma_c) \gamma_c M_c^2}{(1 - \gamma_c) + 2 \gamma_c M_c^2} \right]^{0.5} \times J \quad (2)$$

where H_{mid}/D represents the height of the midpoint of Mach disc non-dimensionalised by the diameter of the jet hole.

Although several experimental studies have been carried out to understand the JISC, there is still a deficiency of experimental data that can be used for the purpose of validation/verification of CFD codes. Recently, Santiago and Dutton [3] carried out experiments on a sonic jet in a cross-flow of Mach 1.6 and measured all three velocity components (U , V , W) and five Reynolds stresses

using Laser Doppler Velocimeter (LDV). As the measurements were taken in several planes, and the accuracy of the measurement technique is considered very good (i.e., LDV method), it provides an excellent opportunity for CFD code validation. Kawai & Lele [2, 29] performed an LES of this JISC experiment and their results were found to be in very good agreement with the experiment. In this paper, an ILES based Godunov type [1] fifth-order spatially accurate method, with variable extrapolation [11], has been used on a structured grid to reproduce the Santiago & Dutton experiment. The present results are compared with the experiment and the classical LES of Kawai & Lele. In the experiment a turbulent boundary layer was developed for the main flow on the flatplate, therefore in the current work a digital-filters based turbulent inflow data generation method [12, 13] has been employed to generate turbulence in the inflow data for the simulations. This method of generating synthetic turbulent inflow conditions satisfies the specified integral length scales and is also very efficient from a computational point of view.

2 Computational Framework

The computational study is based on the CFD code CNS3D [5, 6, 9]. The code utilises different Riemann solvers [7, 8], including flux vector splitting methods, a characteristics-based scheme and the HLLC Riemann solver. In the present study, the HLLC Riemann solver of [22] is used, which assumes a three-wave structure of the Riemann problem solution, allowing for two intermediate states enclosed by the two fastest waves. The HLLC Riemann solver does not use linearisation of the equations and works well for low-density problems and sonic points without any fixes. It has been successfully used to simulate a variety of flows in conjunction with the CNS3D code [5, 6, 30]. The time integration is obtained by an explicit Runge-Kutta scheme third-order accurate [10].

2.1 Governing Equations

The work presented in this paper employs the 3D Navier-Stokes (NS) equations that govern the mechanics of flow of (Newtonian) fluids. The NS equations for the conservation of mass, momentum and energy can be written as:

$$\begin{aligned} \frac{\partial \rho}{\partial t} + \nabla \cdot (\rho \mathbf{u}) &= 0 \quad , \\ \frac{\partial (\rho \mathbf{u})}{\partial t} + \nabla \cdot (\rho \mathbf{u} \mathbf{u}) &= -\nabla \cdot \mathbf{S} \quad , \\ \frac{\partial e}{\partial t} + \nabla \cdot (e \mathbf{u}) &= -\nabla \cdot (\mathbf{S} \cdot \mathbf{u}) - \nabla \cdot \mathbf{q} \quad , \end{aligned} \quad (3)$$

where ρ , e , \mathbf{u} and \mathbf{q} are the density, total energy per unit volume, the velocity components and the heat flux, respectively. The stress tensor \mathbf{S} in Eq. 3 is given by:

$$\mathbf{S} = p(\rho, T) \mathbf{I} + \frac{2}{3} \mu (\nabla \cdot \mathbf{u}) \mathbf{I} - \mu \left[(\nabla \mathbf{u}) + (\nabla \mathbf{u})^T \right] \quad (4)$$

where $p(\rho, T)$, \mathbf{I} , T and μ are pressure, the identity tensor, temperature and dynamic viscosity, respectively. The system of equations is closed using an equation of state:

$$p = \rho R T \quad (5)$$

where, R is the gas constant. The NS equations can be non-dimensionalised and written in matrix form for a rectangular co-ordinate's system; subsequently, the coordinates are transformed to a curvilinear co-ordinate's system to allow for body-fitted grids (for details see [21]).

2.2 Numerical Methods

The work presented in this paper employs the HLLC approximate Riemann solver [22] and higher order spatial accuracy is achieved using the MUSCL extrapolation [23]:

$$\begin{aligned} \mathbf{U}_{i+\frac{1}{2}}^L &= \mathbf{U}_i + \frac{1}{2} \left[\phi^{lim} \left(r^{lim,L} \right) (\mathbf{U}_i - \mathbf{U}_{i-1}) \right] \quad , \\ \mathbf{U}_{i+\frac{1}{2}}^R &= \mathbf{U}_{i+1} - \frac{1}{2} \left[\phi^{lim} \left(r^{lim,R} \right) (\mathbf{U}_{i+2} - \mathbf{U}_{i-1}) \right] \quad , \end{aligned} \quad (6)$$

where, the integer i represents the cell numbers and the ratio of the slopes (r) is defined as:

$$\begin{aligned} r_i^{lim,L} &= \frac{\mathbf{U}_{i+1} - \mathbf{U}_i}{\mathbf{U}_i - \mathbf{U}_{i-1}} , \\ r_i^{lim,R} &= \frac{\mathbf{U}_{i+1} - \mathbf{U}_i}{\mathbf{U}_{i+2} - \mathbf{U}_{i+1}} , \end{aligned} \quad (7)$$

The fifth order slope limiter used is as follows:

$$\begin{aligned} \phi_{M5,L}^{*lim} &= \frac{-2/r_{i-1}^{lim,L} + 11 + 24r_i^{lim,L} - 3r_i^{lim,L}r_{i+1}^{lim,L}}{30} , \\ \phi_{M5,R}^{*lim} &= \frac{-2/r_{i-1}^{lim,R} + 11 + 24r_i^{lim,R} - 3r_i^{lim,R}r_{i+1}^{lim,R}}{30} , \end{aligned} \quad (8)$$

Monotonicity is maintained by taking:

$$\begin{aligned} \phi_{M5,L}^{lim} &= \max\left(0, \min\left(2, 2r_i^{lim,L}, \phi_{M5,L}^{*lim}\right)\right) , \\ \phi_{M5,R}^{lim} &= \max\left(0, \min\left(2, 2r_i^{lim,R}, \phi_{M5,R}^{*lim}\right)\right) , \end{aligned} \quad (9)$$

Guillard *et al.* [26] demonstrated an incorrect pressure difference scaling for low Mach numbers for standard Godunov schemes and Thornber *et al.* [11] presented a theoretical analysis of the large velocity jumps at the cell interfaces and presented a low Mach treatment for the excessive numerical dissipation. It was proposed that the velocity jumps at the cell interfaces should be modified by a function z which gives the reconstructed velocities \mathbf{u} :

$$\begin{aligned} \mathbf{u}_{L,M5+LM} &= \frac{\mathbf{u}_L + \mathbf{u}_R}{2} + z \frac{\mathbf{u}_L - \mathbf{u}_R}{2} , \\ \mathbf{u}_{R,M5+LM} &= \frac{\mathbf{u}_L + \mathbf{u}_R}{2} + z \frac{\mathbf{u}_R - \mathbf{u}_L}{2} , \end{aligned} \quad (10)$$

Finally, the time integration is achieved using the third-order Runge-Kutta scheme [10, 21]:

$$\mathbf{U}_i^1 = \mathbf{U}_i^n + \frac{1}{2} \frac{\Delta t}{\Delta x} f(\mathbf{U}_i^n) ,$$

$$\begin{aligned} \mathbf{U}_i^2 &= \mathbf{U}_i^n + \frac{1}{2} \frac{\Delta t}{\Delta x} [f(\mathbf{U}_i^1)] , \\ \mathbf{U}_i^{n+1} &= \frac{1}{3} \left(2\mathbf{U}_i^2 + \mathbf{U}_i^n + \frac{\Delta t}{\Delta x} [f(\mathbf{U}_i^2) + f(\mathbf{U}_i^1)] \right) , \end{aligned} \quad (11)$$

3 Computations and Results

3.1 Computational Domain and Initialisation

The experiment [3, 4] was effectively carried out on a flat plate with a circular injection port that allowed the gaseous air to emerge into the main stream flow. The initial conditions prescribed for the simulations are the same as the stagnation conditions used for the experiment and are tabulated in Table 1. Note that the Reynolds number used is small when compared with the experiment. This is to allow reasonable resolution of the computational domain and also to match the initial conditions used for the LES by Kawai & Lele [2]. The velocity profile from the experiment, obtained at $x/D=-5$ for a fully developed supersonic turbulent boundary layer, are applied at the $x/D=-8$ position ($x/D=0$ is the centre of the injection hole) in the computational domain as shown in Fig. 2. The long upstream domain is to allow for the weak shock developed at the start of the computational domain. Nevertheless, the turbulent boundary layer profile from the experiment at $x/D=-5$ is matched with the turbulent boundary layer profile at $x/D=-5$ of the computational domain, as shown in Fig. 3(a). Although the Reynolds number used is small, the thickness of the turbulent boundary layer ($\delta_{99}/D = 0.775(3.1mm)$) has been matched at the $x/D=-5$ position in the experiment. The momentum flux ratio (J) is calculated to be 1.7, which also matches the experimental data.

3.2 Results and Analysis

First of all, we examine the flow structure generated when a transverse sonic jet of fluid emerges into a stream of Mach 1.6 turbulent flow. As the under-expanded sonic jet enters the main-stream flow, it acts as a cylindrical obstruction to the

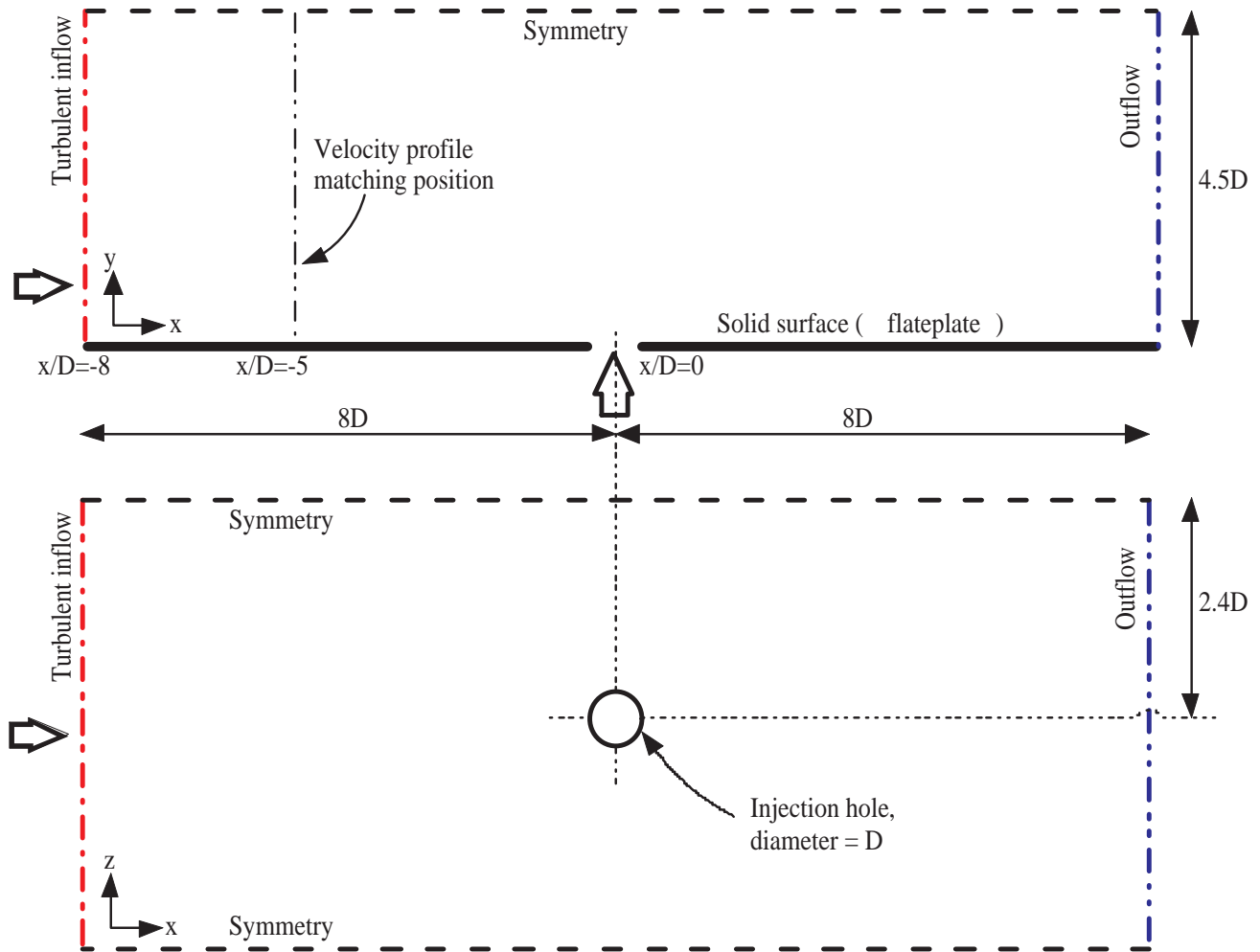


Fig. 2 Schematic diagram of the computational domain selected for the JISC simulations indicating various boundary conditions employed to the domain.

Table 1 Average stagnation inflow conditions from experiment[3], c and j stand for cross-flow and jet, respectively.

| Property | Value | Units |
|-----------------------|----------------|-------|
| Mach Number (c) | $1.59 \pm 1\%$ | |
| Mach Number (j) | 1.0 | |
| Stag. Pressure (c) | 241 | kPa |
| Stag. Pressure (j) | 476 | kPa |
| Stag. Temperature (c) | 295 | K |
| Stag. Temperature (j) | 295 | K |
| Average Velocity (c) | 446.1 | m/s |
| Reynolds Number | $2.4E+04$ | |

main-stream flow. This gives rise to a bow shock ahead of the injection. This bow shock in turn results in a large pressure gradient behind the shock and a separation zone is generated on the flat plate just ahead of the jet plume. This separation zone also produces a lambda shock and is a comparatively large separation zone (“R.Z.:1”) as shown in Fig. 4. Another small separation zone ahead of the injection is also identified in the experiment of Santiago & Dutton [3], which has been successfully captured in the current simulations, shown in Fig. 4 as “R.Z.:2”. There is a third separation zone “R.Z.:3” clearly visible in the flow structure behind the plume, which is also identified in the experiment. As the jet emerges

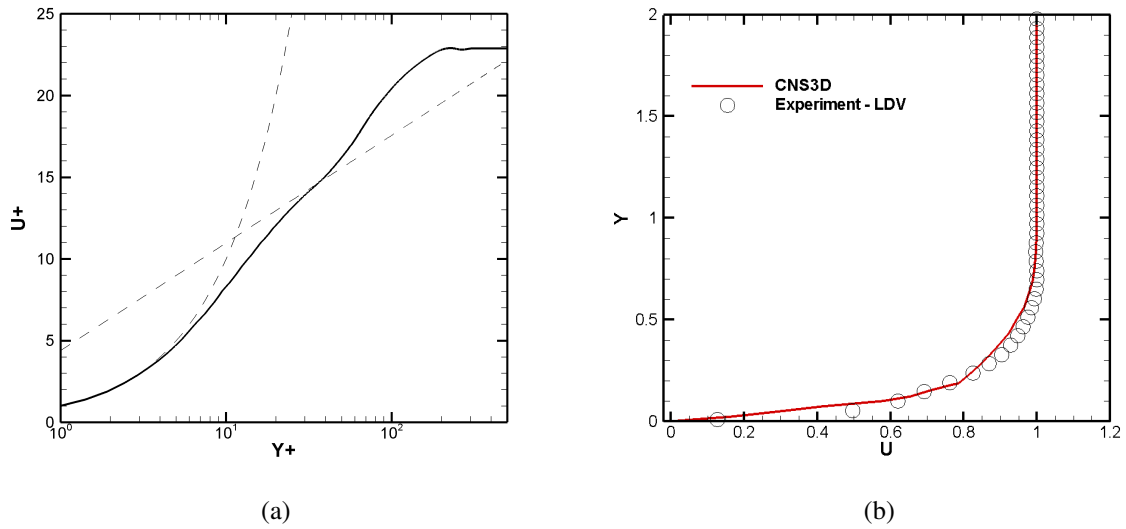


Fig. 3 (a) Non-dimensional velocity versus the non-dimensional wall distance (log) plot for the inflow turbulent boundary layer at $x/D=-5$. (b) velocity profile for the inflow turbulent boundary layer at $x/D=-5$ match with the experimental velocity profile at the same position.

into the main-stream flow, it expands and turns along the main flow at the same time as shown by the Prandtl-Meyer expansion fan in Fig. 4. The boundary of the jet that forms the barrel shock and the Mach disc meets at a point referred to

as the triple point. There are also present in the flow structure the horseshoe vortex and a pair of counter-rotating vortices which will be discussed later. The penetration of the jet into the main-stream flow has been measured to be $\approx 1.4D$ as

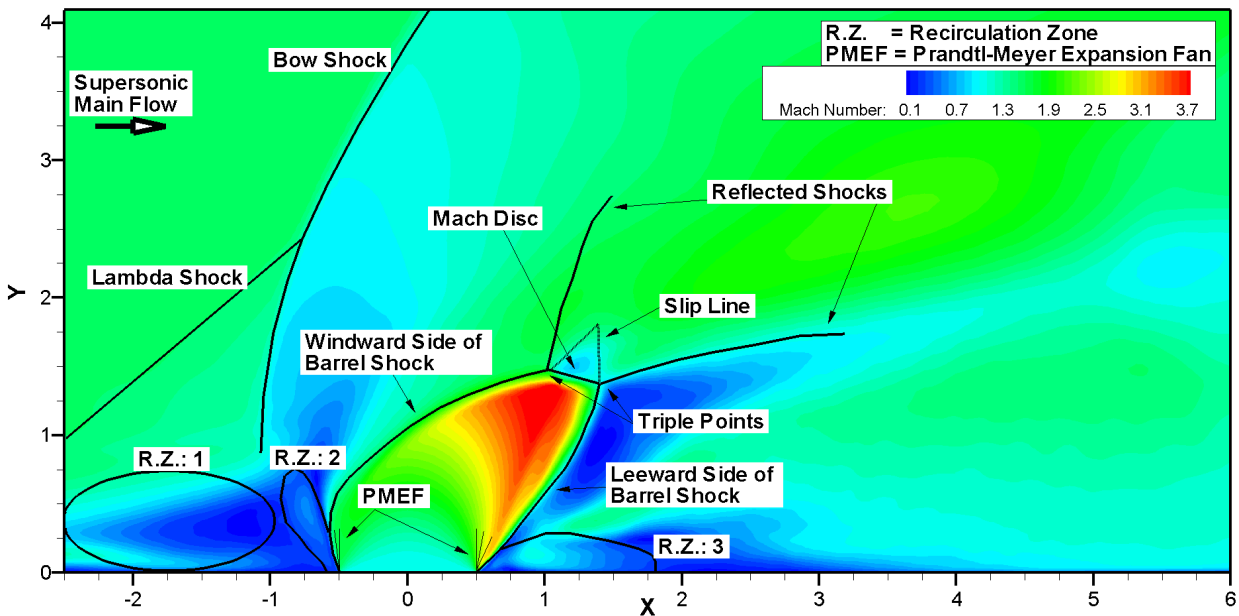


Fig. 4 JISC flow structure at middle z -plane, ($z/D=0$), typical shocks and flow features are identified as the sonic jet mixes with transverse supersonic flow at Mach 1.6

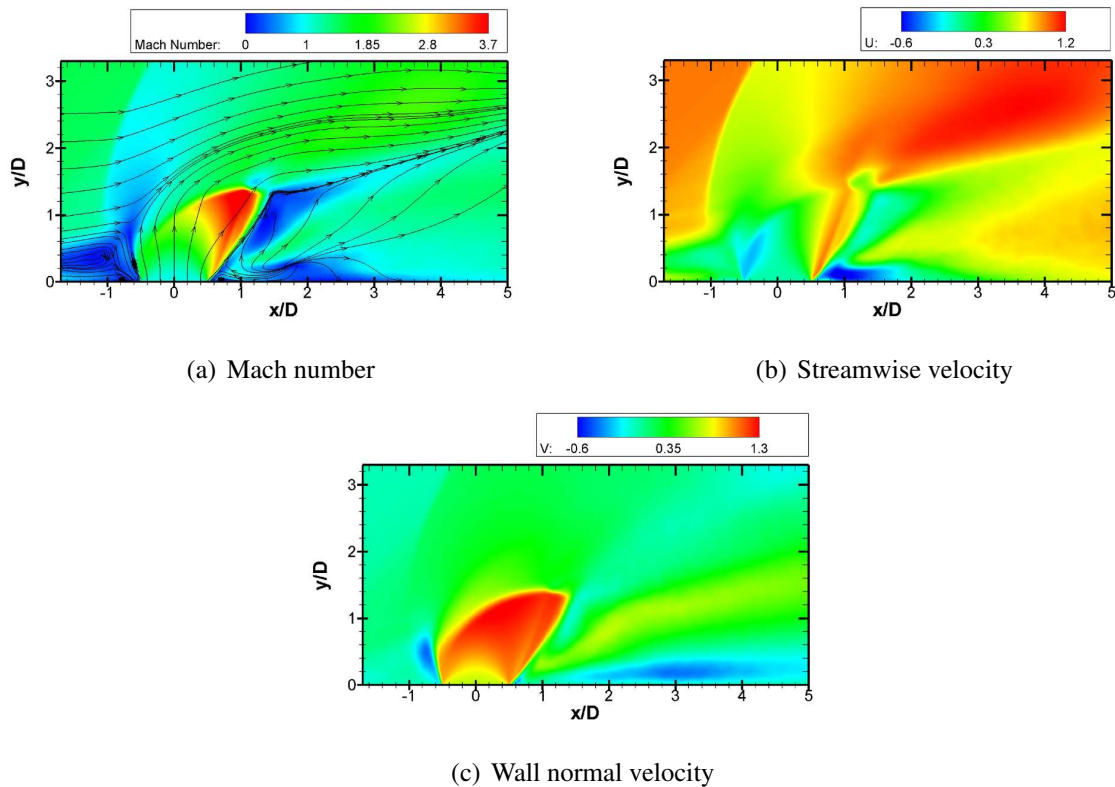


Fig. 5 Time averaged Mach number, streamwise and wall normal velocity contours at the z -plane ($z/D=0$) showing typical flow structure with JISC at Mach 1.6

calculated using Eq. 2. The flow analysis carried out in this work is time averaged over the period for the main-stream flow to go through the whole geometry 5 times.

Figure 5 shows the time averaged Mach number, streamwise velocity and wall normal velocity distributions in the midline transverse plane, i.e. $z/D=0$. The contour plots show the complete shock structures with JISC at Mach 1.6 such as lambda shock, bow shock, barrel shock, Mach disc and the separation zones. The stream lines show the flow of the fluid just upstream and downstream of the plume up to a distance of $x/D=5$. As the main-stream flow approaches the plume and the bow shock is developed, the Mach number and the velocities exhibit sharp deceleration just ahead of the plume and a rapid acceleration is found in the plume towards the top edge region. Thus, the maximum Mach number is found at the top edge of the plume which conforms with the experimental results. Most of the jet fluid passes through the windward side of the

plume and the Mach disc. It is understood from the instantaneous flow visualisation that this is the region where the mixing of the fluids takes place largely. The recirculation region just ahead of the plume and below the bow shock develops sideways of the plume and forms the well known horseshoe vortices around the plume.

Considering the flow analysis in the plane parallel to the wall, Fig. 6 shows the time averaged contours of the Mach number, streamwise velocity and wall normal velocities at $y/D=1$ (y -plane). The sudden deceleration just ahead of the jet plume and acceleration within the jet plume is clearly shown in these views as well. The stream-lines on the Mach number plots show the flow turning sideways as it approaches the jet plume and thus forms the horseshoe vortex around it. Just after the jet plume a low velocity region is visible. In respect of the separation area behind the jet plume (Figs. 5 and 6), two small trailing vortices emerge which will be seen clearly in the cross-view planes shown in Figs. 7-9.

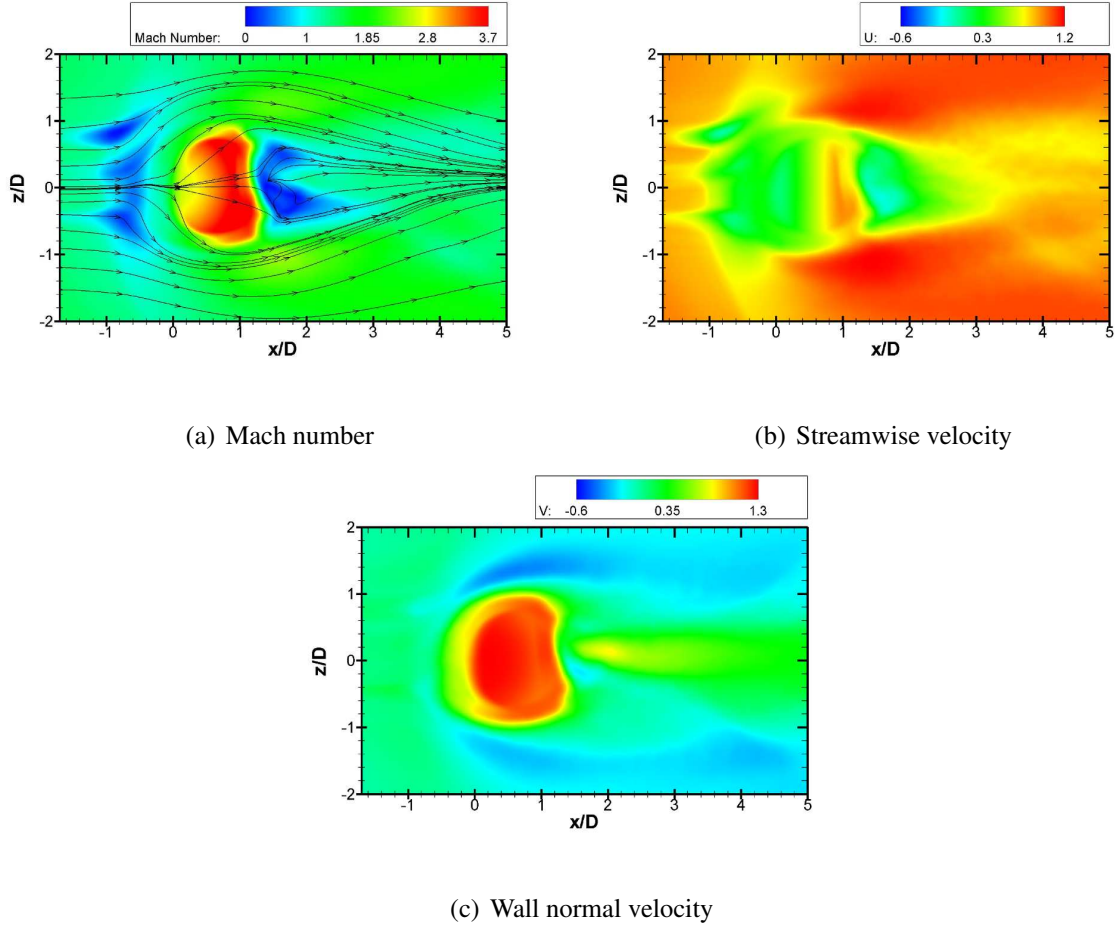


Fig. 6 Time averaged Mach number, streamwise and wall normal velocity contours at the wall parallel y -plane ($y/D=0$) showing typical flow structure with JISC at Mach 1.6

Figures 7, 8 and 9 show the cross-planes at three different locations of $x/D=1, 3,$ and 5 for the Mach number, streamwise and wall-normal velocities. The complete 3D structure of the time averaged JISC flow field is best understood by combining and analysing all the three figures. The $x/D=1, 3,$ and 5 planes are just downstream of the jet plume and the plots show the development of the two well known counter-rotating vortices (CRVs). The figures also show streamlines which enhance the visualisation of the pair of CRVs and how they are developing. It can be seen from the $x/D=3$ plot that a pair of small vortices also develop below the main pair of CRVs and close to the wall. This occurs as a result of the flow separation just after the jet injection position i.e., “R.Z.:3” as shown in Fig. 4. These transient vortices and the large counter rotating

pair of vortices enhance the mixing mechanism of the fluids in the downstream region. It is also noticed from these plots that the pair of CRVs gains height very quickly after the full jet penetration is achieved. After this point the height of this pair of CRVs remains more-or-less constant but the diameter increases which again refers to the better mixing of the fluids.

The flow properties are then analysed for the mean streamwise and wall-normal velocities at various points and compared with the experimental and LES results from the recently published work of Kawai and Lele [2]. It should be mentioned that the present results have been obtained using almost one-third of the resolution of previous LES [2, 29]. Figures 10 and 11 show the plots for the mean streamwise and wall-normal velocities, respectively, at various positions up-

Investigation of Sonic Jet Mixing in a Stream of Supersonic Cross-flow Using Large Eddy Simulations

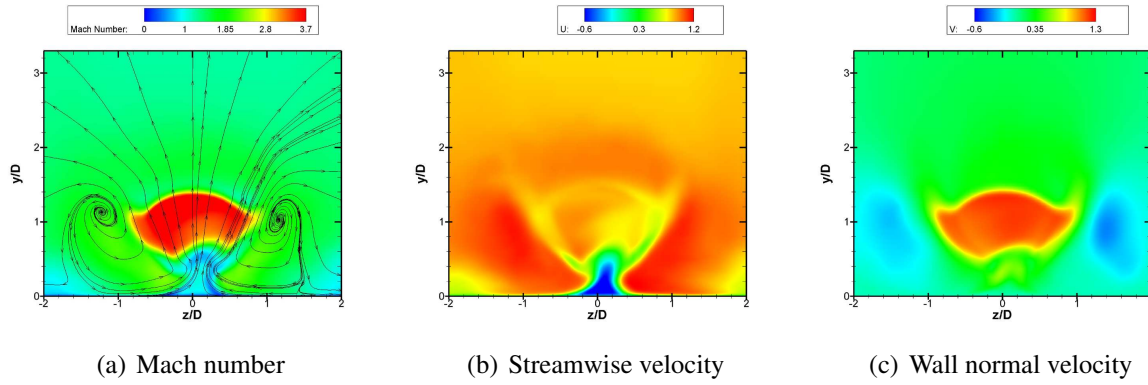


Fig. 7 Time averaged Mach number, streamwise and wall normal velocity contours at the cross-view x -plane ($x/D=1$) showing typical flow structure with JISC at Mach 1.6 along with the CRV.

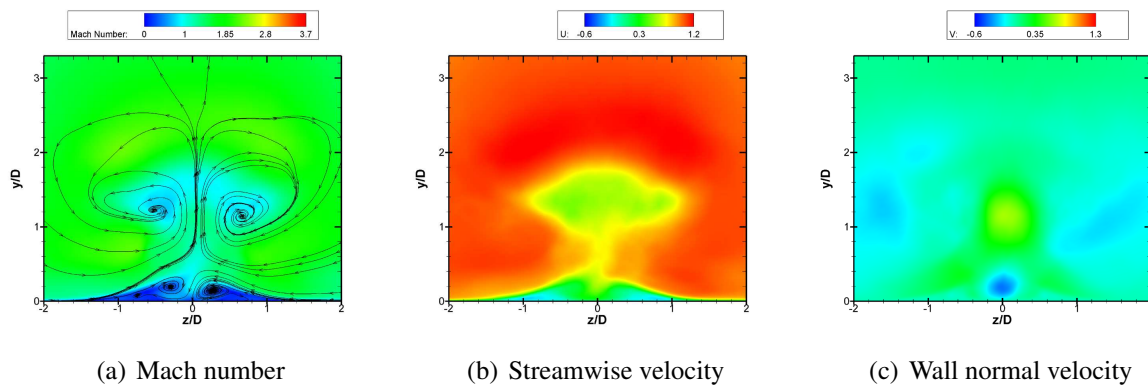


Fig. 8 Time averaged Mach number, streamwise and wall normal velocity contours at the cross-view x -plane ($x/D=3$) showing typical flow structure with JISC at Mach 1.6 along with the CRV.

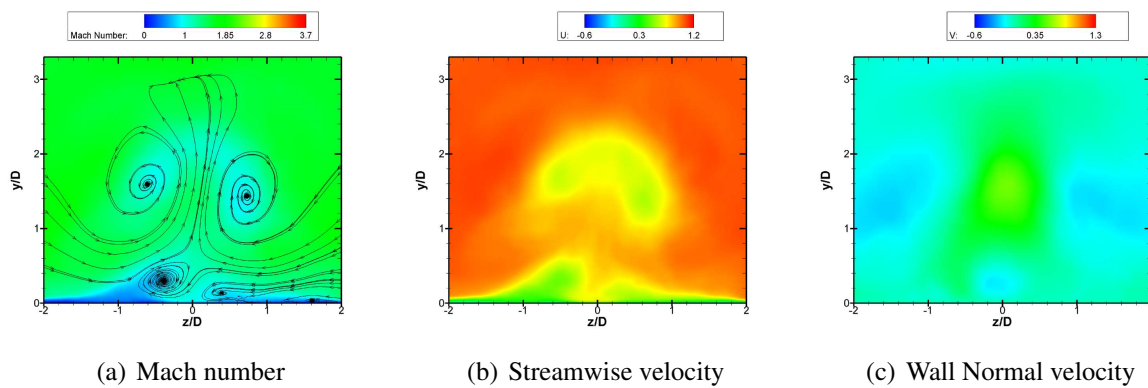


Fig. 9 Time averaged Mach number, streamwise and wall normal velocity contours at the cross-view x -plane ($x/D=5$) showing typical flow structure with JISC at Mach 1.6 along with the CRV.

stream and downstream of the jet plume. Upstream of the jet, the flow is influenced by turbulence in the inflow conditions. It has been presented [2] that the upstream flow properties at po-

sition $x/D=-1$ are different for laminar and turbulent flow. It has been noticed that in the case of turbulent flow the weak lambda shock develops quite close to the bow shock and maintains its po-

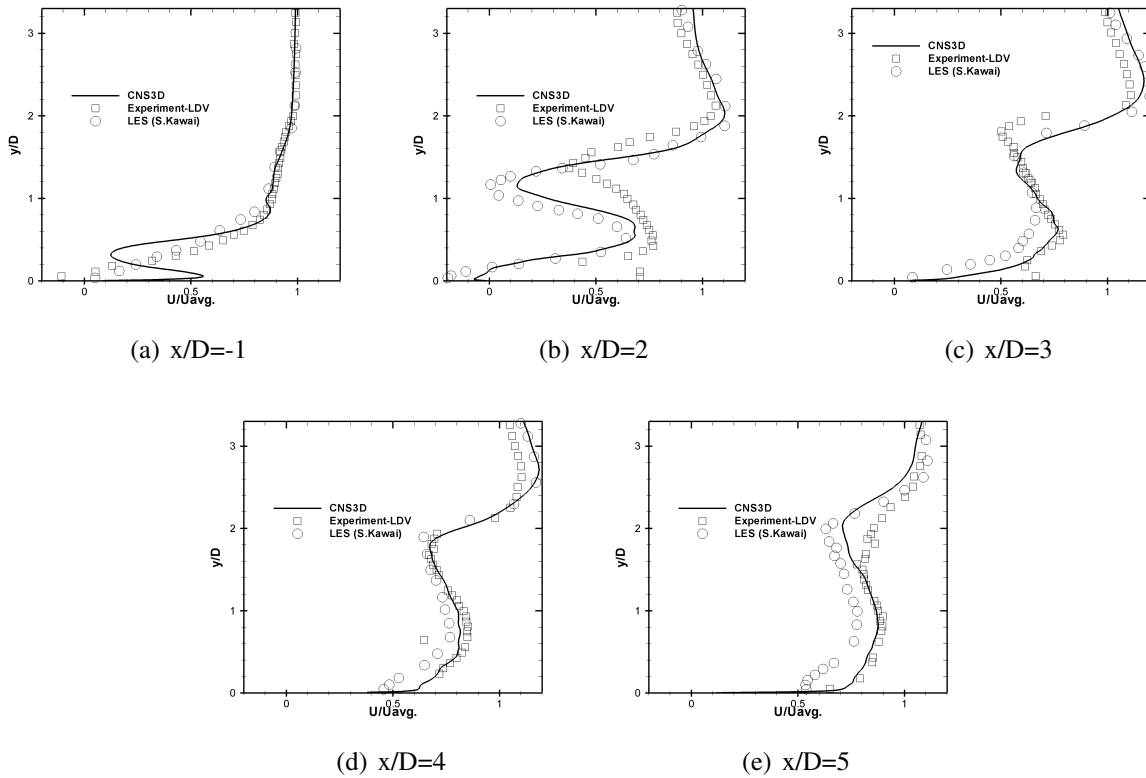


Fig. 10 Time averaged streamwise velocity profiles at various positions on the midline z -plane ($z/D=0$); comparison with the experiments [3, 4] and LES [2, 29].

sition. This causes the slight jump in the streamwise and wall-normal velocities as shown in Figs. 10(a) and 11(a) near the position $y/D \approx 2$. Comparing the velocity profiles downstream of the jet it can be noticed that very close to the jet the averaged streamwise velocity profile (at $x/D=-1$ and 2) is slightly over-predicted. This can be due to the fact that this area on both sides of the jet comprise the separation zones. But looking at the previous LES results, we find the same trend in the previous work as well. Apart from this, all the other positions compare well with the experimental results, especially at the $x/D=5$ position where a very good agreement between the experiment, previous LES, and current work is found.

Further analysis is carried out for the mean pressure distributions on the wall upstream and downstream the jet injection hole. The experiment was conducted by Everett *et al.* [28] using a Pressure Sensitive Paint (PSP) technique. Figure 12 shows the comparison of the mean pressure

distribution on the wall when compared with the experiment and the previous LES. Figure 12(a) shows a very good comparison between all three results. However, in Fig. 12(c) some discrepancy is found in the results from the current study. It is believed that this could be due to very coarse grid resolution far away at the $z/D=2$ location. But looking at the results of Fig. 12 (a) & (b), which shows the pressure distributions at locations $z/D=0$ and 1, it can be said that by using a finer resolution a better result can be obtained at the $z/D=2$ location as well.

4 Concluding remarks

ILES results for transverse jet injected into a supersonic cross-flow were presented and compared with experimental data and classical LES results, showing an overall very good agreement. The present ILES was performed using almost one-third of the resolution of the classical LES. The simulated flow structures show very good

Investigation of Sonic Jet Mixing in a Stream of Supersonic Cross-flow Using Large Eddy Simulations

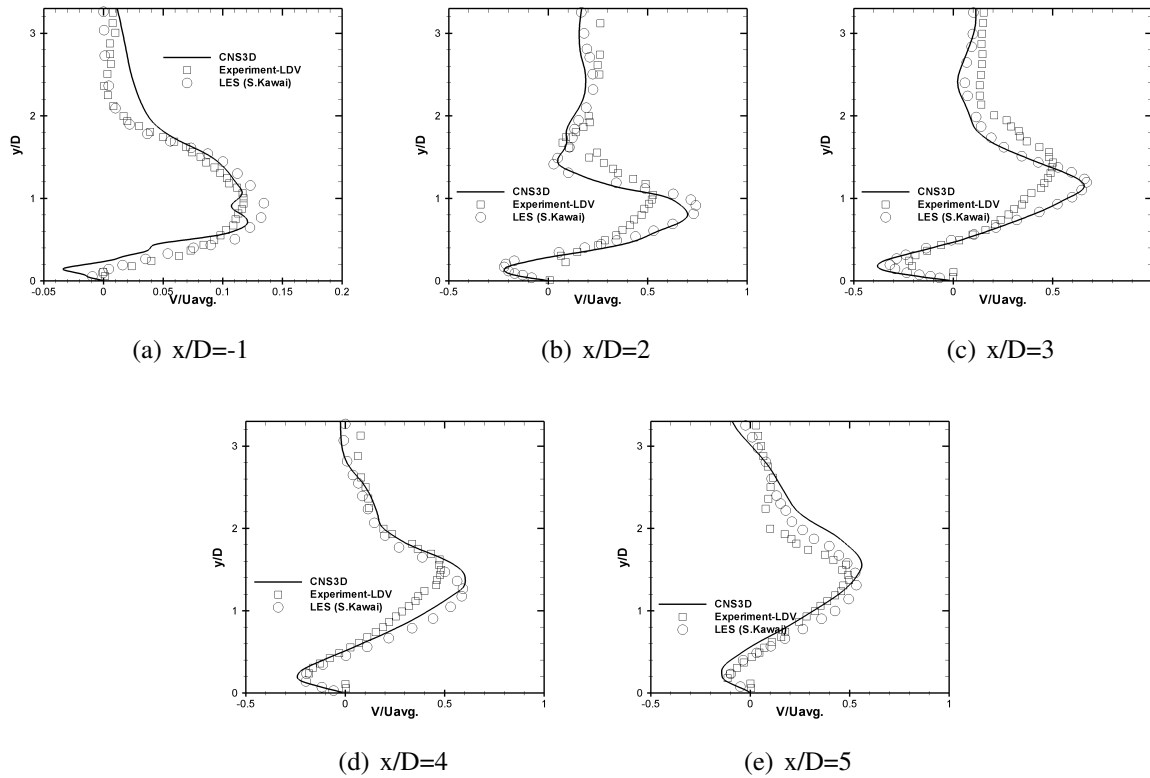


Fig. 11 Time averaged wall normal velocity profiles at various positions on the midline z -Plane ($z/D=0$); comparison with the experiments [3, 4] and LES [2, 29].

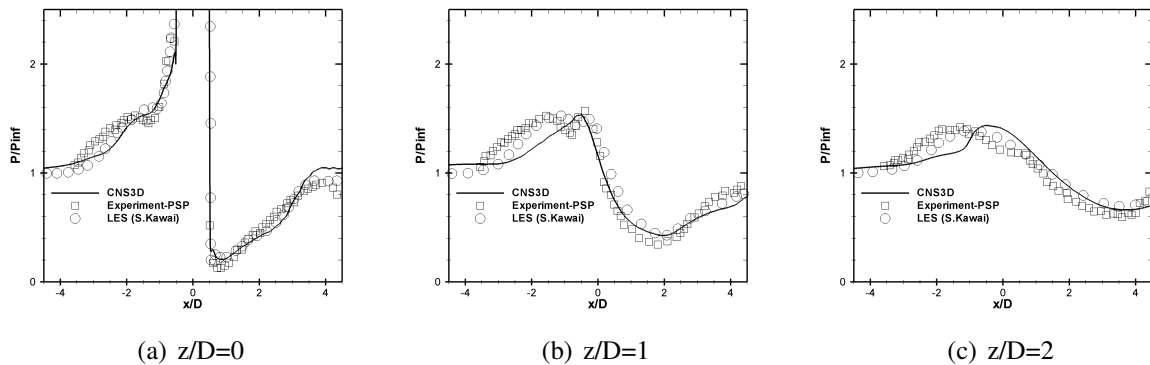


Fig. 12 Time averaged pressure profiles at various positions on the wall parallel y -Plane ($y/D=1$); comparison with the experiments [28] and LES [2, 29].

agreement with the well established understanding of JISC as all the flow features have been captured well. It is understood from previous work [29] that turbulent inlet flow can largely influence the flow properties upstream of the jet plume. Downstream of the jet plume the flow properties remain largely unaffected by the turbulent in-

flow. Further analysis is required into the turbulent kinetic energy and Reynolds stresses, with and without imposing a turbulent inflow, in order to better understand the effects of the initial and boundary conditions.

5 Acknowledgements

The authors would like to acknowledge Dr Emile Touber (Imperial College, London, U.K.) and Dr Soshi Kawai (Stanford University, Stanford, CA, USA) for their advice.

5.1 Copyright Statement

The authors confirm that they, and/or their company or organization, hold copyright on all of the original material included in this paper. The authors also confirm that they have obtained permission, from the copyright holder of any third party material included in this paper, to publish it as part of their paper. The authors confirm that they give permission, or have obtained permission from the copyright holder of this paper, for the publication and distribution of this paper as part of the ICAS2010 proceedings or as individual off-prints from the proceedings.

5.2 Contact Author Email Address

The corresponding author can be contacted by email at the following address: z.a.rana@cranfield.ac.uk

References

- [1] Godunov S. A finite-difference method for the computation of discontinuous solutions of the equations of fluid dynamics. *Mat. Sb.* vol. 47, pp. 271-295, 1959.
- [2] Kawai S and Lele S. Large-eddy simulation of jet mixing in a supersonic turbulent crossflow. *19th AIAA Computational Fluid Dynamics.* 22 - 25 June 2009, San Antonio, Texas, (AIAA-2009-3795).
- [3] Santiago J and Dutton J. Velocity measurements of a jet injected into a supersonic flow. *Journal of Propulsion and Power.* Vol. 13, no. 2, March-April 1997
- [4] VanLerberghe W, Santiago J, Dutton J, and Lucht R. Mixing of a sonic transverse jet injected into a supersonic flow. *AIAA Journal.* Vol. 38, iss. 3, March 2000
- [5] Drikakis, D., Tsangaris, S., "Real Gas Effects for Compressible Nozzle Flow," *ASME Journal of Fluid Engineering,* Vol. 115, pp. 115-120, 1993.
- [6] Drikakis, D., Tsangaris, S., "On the Accuracy and Efficiency of CFD Methods in Real Gas Hypersonics," *International Journal for Numerical Methods in Fluids,* Vol. 16, pp. 759-775, 1993.
- [7] Drikakis, D. "Advances in turbulent flow computations using high-resolution methods," *Progress in Aerospace Science,* 39, 405-424, 2003.
- [8] Bagabir, A., and Drikakis, D., "Numerical Experiments Using High-Resolution Schemes for Unsteady, Inviscid, Compressible Flows," *Computer Methods in Applied Mechanics and Engineering,* Vol. 193, March. 2004, pp. 4675-4705.
- [9] Zoltak, J., and Drikakis, D., "Hybrid Upwind Methods for the Simulation of Unsteady Shock-Wave Diffraction Over a Cylinder" , *Computer Methods in Applied Mechanics and Engineering,* Vol. 162, Oct. 1998, pp. 165-185.
- [10] D. Drikakis, M. Hahn, A. Mosedale, and B. Thornber. Large eddy simulation using high-resolution and high-order methods. *Phil. Trans. R. Soc. A,* 367(1899):29852997, 2009.
- [11] Thornber B, Drikakis D, Williams R, Mosedale A, and Youngs D. An improved reconstruction method for compressible flows with low Mach number features. *J. Comp. Phys.* Vol. 227, iss. 10, 2008, pp. 4873-4894.
- [12] Xie Z and Castro I. Efficient generation of inflow conditions for large eddy simulation of street-scale flows. *Flow Turbulence Combust.* (2008) 81:449-470 DOI 10.1007/s10494-008-9151-5
- [13] Touber E and Sandham N. Large-eddy simulation of low-frequency unsteadiness in a turbulent shock-induced separation bubble. *Theor. Comput. Fluid Dynamics.* Vol.23: 79-107 (2009) DOI 10.1007/s00162-009-0103-z
- [14] Gruber M, Nejad A, Chen T and Dutton J. Mixing and penetration studies of sonic jets in a Mach 2 freestream. *Journal of Propulsion and Power.* Vol. 11, No. 2, 1995, pp. 315-323.
- [15] Ben-Yakar A, Mungal G and Hanson R. Time evolution and mixing characteristics of hydrogen and ethylene transverse jets in supersonic crossflows. *Physics of Fluids.* Vol. 18, No. 2, February 2006.
- [16] Admason T and Nicholls J. On the structure of jets from highly underexpanded nozzles into still air. *Journal of the Aerospace Sciences.* Vol. 26, No. 1, 1958, pp. 16-24.

- [17] Love E and Grigsby C. Some studies of a symmetric free jets exhausting from sonic and supersonic nozzles into still air and into supersonic streams. *NACA Report RM-L54L31*. 1955.
- [18] Billig F, Orth R and Lasky M. A unified analysis of gaseous jet penetration. *AIAA Journal*. Vol. 9, No. 6, 1971.
- [19] Cohen L, Coulter L and Egan W. Penetration and mixing of multiple gas jets subjected to a cross flow. *AIAA Journal*. Vol. 9, No. 4, April 1971.
- [20] Schetz J and Billig F. Penetration of gaseous jets injected into a supersonic stream. *Journal of Spacecraft*. Vol. 3, No. 11, November 1966.
- [21] Drikakis D and Rider W. *High-Resolution Methods for Incompressible and Low-Speed Flows*. Springer-Verlag, Berlin, 2005.
- [22] Toro E. *Riemann Solvers and Numerical Methods for Fluid Dynamics*. Springer-Verlag, 2009.
- [23] Van-Leer B. Towards the ultimate conservative difference scheme-IV. A new approach to numerical convection. *Journal of Comp. Phys.* Vol. 23, 1977, pp. 276-299.
- [24] Hahn M. Implicit large-eddy simulation of low-speed separated flows using high-resolution methods. *PhD thesis, School of Engineering, Cranfield University, Cranfield, U.K.* 2008.
- [25] Thornber B. Implicit large eddy simulation for unsteady multi-component compressible turbulent flows. *PhD thesis, School of Engineering, Cranfield University, Cranfield, U.K.* 2007.
- [26] Guillard H and Murrone A. On the behaviour of upwind schemes in the low Mach number limit: II. Godunov type schemes. *Computers & Fluids* vol. 33, iss. 4, 2004, pp. 655-675.
- [27] Thornber B, Drikakis D, Williams R, Mosedale A, and Youngs D. An improved reconstruction method for compressible flows with low Mach number features. *Journal of Comp. Phys.* vol. 227, iss. 10, 2008, pp. 4873-4894.
- [28] Everett D, Woodmansee M, Dutton J, and Morris M. Wall pressure measurements for a sonic jet injected transversely into a supersonic cross flow. *Journal of Propulsion and Power*. vol. 14, iss. 6, 1998, pp. 861-868.
- [29] Kawai S and Lele S. Large-eddy simulation of jet mixing in supersonic turbulent crossflows. *To be Published or In Printing; AIAA Journal*. DOI: 10.2514/1.J050282 .
- [30] Rana, Z.A., Thornber, B.J.R, and Drikakis, D., "Large Eddy Simulation of a Scramjet Model (HyShot-II) Using High-Resolution Methods", *45th AIAA/ASME/SAE/ASEE Joint Propulsion Conference & Exhibit*. 2-5 Aug. 2009, Denver, CO.